

Atomic Force Microscopy and MD Simulations Reveal Pore-Like Structures of All-D-Enantiomer of Alzheimer's β -Amyloid Peptide: Relevance to the Ion Channel Mechanism of AD Pathology

Laura Connelly,^{†,⊥} Hyunbum Jang,^{‡,⊥} Fernando Teran Arce,[†] Ricardo Capone,[†] Samuel A. Kotler,[†] Srinivasan Ramachandran,[†] Bruce L. Kagan,[§] Ruth Nussinov,^{*,‡,||} and Ratnesh Lal^{*,†}

[†]Departments of Bioengineering and of Mechanical and Aerospace Engineering and Materials Science Program, University of California, San Diego, La Jolla, California 92093, United States

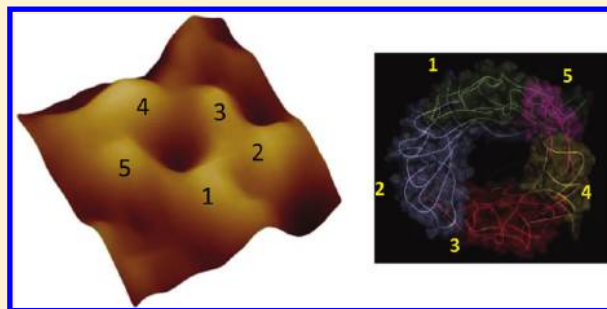
[‡]Center for Cancer Research Nanobiology Program, SAIC-Frederick, Inc., NCI-Frederick, Frederick, Maryland 21702, United States

[§]Department of Psychiatry, David Geffen School of Medicine, Semel Institute for Neuroscience Human Behavior, University of California, Los Angeles, California 90024, United States

^{||}Department of Human Molecular Genetics and Biochemistry, Sackler School of Medicine, Tel Aviv University, Tel Aviv 69978, Israel

S Supporting Information

ABSTRACT: Alzheimer's disease (AD) is a protein misfolding disease characterized by a buildup of β -amyloid ($A\beta$) peptide as senile plaques, uncontrolled neurodegeneration, and memory loss. AD pathology is linked to the destabilization of cellular ionic homeostasis and involves $A\beta$ peptide–plasma membrane interactions. In principle, there are two possible ways through which disturbance of the ionic homeostasis can take place: directly, where the $A\beta$ peptide either inserts into the membrane and creates ion-conductive pores or destabilizes the membrane organization, or, indirectly, where the $A\beta$ peptide interacts with existing cell membrane receptors. To distinguish between these two possible types of $A\beta$ -membrane interactions, we took advantage of the biochemical tenet that ligand–receptor interactions are stereospecific; L-amino acid peptides, but not their D-counterparts, bind to cell membrane receptors. However, with respect to the ion channel-mediated mechanism, like L-amino acids, D-amino acid peptides will also form ion channel-like structures. Using atomic force microscopy (AFM), we imaged the structures of both D- and L-enantiomers of the full length $A\beta_{1-42}$ when reconstituted in lipid bilayers. AFM imaging shows that both L- and D- $A\beta$ isomers form similar channel-like structures. Molecular dynamics (MD) simulations support the AFM imaged 3D structures. Previously, we have shown that D- $A\beta_{1-42}$ channels conduct ions similarly to their L-counterparts. Taken together, our results support the direct mechanism of $A\beta$ ion channel-mediated destabilization of ionic homeostasis rather than the indirect mechanism through $A\beta$ interaction with membrane receptors.



INTRODUCTION

Alzheimer's disease (AD) is characterized by an aberrant buildup of extracellular protein plaques, uncontrolled neurodegeneration, chronic dementia, and memory loss.^{1–4} AD plaques are predominantly composed of β -amyloid ($A\beta_{1-39-42}$) peptides derived from the proteolytic cleavage of its precursor protein, amyloid precursor protein (APP),^{5,6} and form amyloid structures.⁷ The role of amyloidogenicity in cellular toxicity is unclear, and mounting evidence supports the role of oligomeric $A\beta$.^{8,9} Furthermore, the AD pathology is increasingly believed to be mediated by globular $A\beta$ disrupting the ionic homeostasis through its interaction with cellular membranes.^{10–14} Understanding the interaction of $A\beta$ with the cell membrane and its effects on cellular degeneration is crucial to the understanding of the pathological origin of AD and would eventually aid the prevention and treatment of the disease.

Two mechanisms have been proposed to explain $A\beta$ -mediated toxicity. According to the first, the $A\beta$ peptide forms oligomeric complexes organized as pores, similar to other cytotoxic peptides.¹⁵ Atomic force microscopy (AFM) images support the presence of $A\beta$ channels in lipid bilayers.^{14,16} The activity and function of these channels have been supported by electrophysiological recordings, molecular dynamics (MD) simulations, and cell calcium and degeneration studies.^{17–22} amyloid channels conduct cations, resulting in a gain-of-function type pathological response.^{15,23} According to this mechanism, $A\beta$ inserts directly into the cell membrane and allows cellular Ca^{2+} uptake, thus unbalancing the cell ionic

Received: November 10, 2011

Revised: January 2, 2012

Published: January 4, 2012

homeostasis, which can lead to neurodegeneration.^{10,13,14,24,25} An alternative mechanism for A β -mediated destabilization of ionic homeostasis suggests that the A β peptide interacts with the membrane via stereospecific interactions involving membrane receptors.^{26–28} Several cellular stereospecificity studies related to A β membrane receptors have been reported but with conflicting results.^{27–29} This may be due to variation in cell lines, sample preparation and handling, and most importantly, the lack of any definite single toxic mechanism.

To distinguish between the two mechanisms, we address the question of whether such specific peptide–receptor interaction is a requirement for A β -mediated toxicity. Stereospecificity can be studied through comparison of the biological activities of the L- and D-enantiomers. In a stereospecific receptor–ligand relationship, only L- (and not D-) amino acids are known to interact with membrane receptors. Therefore, the formation of pores in the presence of the D-enantiomer only would suggest that pore formation can take place in the absence of stereospecific interactions, and as such, any cellular effect(s) would result from A β toxic channels directly, without receptors.

To date, there has been no study focusing on the structural stereospecificity of A β ionic channels. We report elsewhere that all the L- and D-amino acids A β _{1–42} isomers (L-A β _{1–42} and D-A β _{1–42}, respectively) exhibit comparable channel conductivity in lipid bilayers.³⁰ Here, using AFM imaging and MD simulations, we present direct structural evidence of the pore-like morphology of the natural L-A β _{1–42} peptide and its mirror image, the D-A β _{1–42} isomer. D-A β _{1–42} retains the properties of its L-analog: the oligomer and fibril formation of the D-A β _{1–42} are indistinguishable from the L-A β _{1–42}.

EXPERIMENTAL METHODS

Materials. For storage, peptides were solubilized in ultrapure water at a concentration of 1 mg/mL, aliquoted, and stored at –80 °C. Aliquots were thawed once and used immediately. After thawing, an appropriate amount of 0.22 μ m filtered NH₄OH solution was added to the aliquot to reach a 1% solution. Molecular Biology grade water from Fisher Scientific (Pittsburgh, PA) was used for sample preparations and Dulbecco's phosphate-buffered saline without Ca²⁺ and Mg²⁺ (Fisher Scientific) was used for AFM imaging in liquid. The phospholipid, 1,2-dioleoyl-*sn*-glycero-3-phosphocholine (DOPC), was purchased from Avanti polar lipids (Alabaster, AL).

AFM Imaging. A multimode AFM equipped with a Nanoscope IIIa controller (Bruker, Santa Barbara, CA) was used. Oxide-sharpened cantilevers with nominal spring constants (k_n) of 0.02 N/m or 0.08 N/m were employed. For experiments performed in liquid, a fluid cell (Bruker) was utilized. Before each experiment, the fluid cell was washed with detergent (~5 min) and vigorously rinsed with constant stream of DI water. The fluid cell was then sonicated for 2 min in molecular grade water, dried with a Kim wipe, and used immediately. Imaging in liquid was performed in phosphate-buffered saline (PBS) without Ca²⁺ and Mg²⁺. Images in liquid were acquired in tapping mode at scan frequencies of 0.5–3.0 Hz and drive amplitudes below 100 mV. The cantilever oscillation frequency was 5–10 kHz. Image analysis was performed using the Bruker Nanoscope software. Some of the AFM images were low-pass filtered to remove noise.

Because the widths of fibers are increased in the AFM images due to tip–sample convolution, we used a simple geometrical deconvolution model to obtain a good estimation of the actual

size of the fiber width, w , from the width, w_0 , observed in the AFM image^{31–33}

$$w_0 - w = 2(2Rh + h^2)^{1/2}$$

Here R is the tip apex radius and h is the height of the fiber. We assumed the tip radius to be 30 nm.³¹

Sample Preparation. Thawed from –80 °C, D- and L-A β _{1–42} aliquots were mixed with 1.01% NH₄OH solution to bring the peptides to a 1% NH₄OH solution. For time-lapse imaging of peptides, these were sonicated for 20 min in an ice bath. New cantilevers or used cantilevers cleaned for 5 min in a UV/ozone chamber (Bioforce Nanosciences, Ames, IA) were utilized for imaging. Freshly cleaved mica was imaged in PBS without Ca²⁺ and Mg²⁺ to check for contamination before the addition of the peptide. The peptide-containing solution was added through the channel of the fluid cell and mixed with a pipet several times. Additional PBS was added as needed to account for evaporation. Samples were kept inside the AFM over the entire span of the experiment. The AFM was maintained at room temperature and covered with parafilm in a semihumid environment to minimize evaporation of the peptide solution.

DOPC bilayers were formed by drying 30 μ L of DOPC (10 mg/mL) dissolved in chloroform in a rotovap and replacing vacuum with Ar. The dried lipid cake was hydrated with 300 μ L (1 mg/mL) of an electrolyte solution containing 150 mM KCl and 1 mM MgCl₂ buffered with 10 mM HEPES, pH 7.4 and vortexed gently. The liposomes formed through this procedure were sonicated for 5 min in an ice bath. Following thawing of the aliquoted peptide solutions, this was brought to a concentration of 1 mg/mL in 1% NH₄OH and sonicated for ~30 s. For incorporation of the peptides in the lipid bilayer, DOPC liposomes and peptide were combined at 20:1 weight ratio and sonicated in an ice bath for 10 min. Liposomes and incorporated peptides were allowed to adsorb on freshly cleaved mica for 30 s to form supported bilayers via rupture and fusion of the reconstituted liposomes. The samples were then washed ten times with PBS buffer (no Ca²⁺ and Mg²⁺) to remove weakly adsorbed peptide or lipid. AFM imaging was subsequently conducted at room temperature.

For fibrils' preparation and imaging, the peptide solutions were thawed and brought to solution concentrations of 1% NH₄OH (1 mg/mL). These were incubated in centrifuge tubes at 37 °C for up to 72 h without mixing. Incubated peptides (1 mg/mL) were allowed to adhere to freshly cleaved mica for 4 min, rinsed gently three times with Molecular Biology grade water, and dried briefly under a stream of N₂.

Molecular Dynamics Simulations. To simulate A β barrels, we used two U-shaped monomer conformations: one is A β _{1–42} as defined in the pentamer based on hydrogen/deuterium-exchange NMR data, side-chain packing constraints from pairwise mutagenesis, and solid-state NMR and EM (PDB code: 2BEG);³⁴ the other is A β _{1–40} based on the solid-state NMR model of small protofibrils.³⁵ However, both conformers miss the N-terminal coordinates due to conformational disorder. We used the N-terminal coordinates obtained from the solution NMR structure of A β _{1–16}; the Zn²⁺ was removed (PDB code: 1ZE7).³⁶ This structure was used to fill in the missing N-terminal portion of the peptides. For each combination of the N-terminal structure with the U-shaped motifs, two A β _{1–42} conformers were generated. Conformer 1 has a turn at Ser26-Ile31, and conformer 2 has a turn at Asp23-

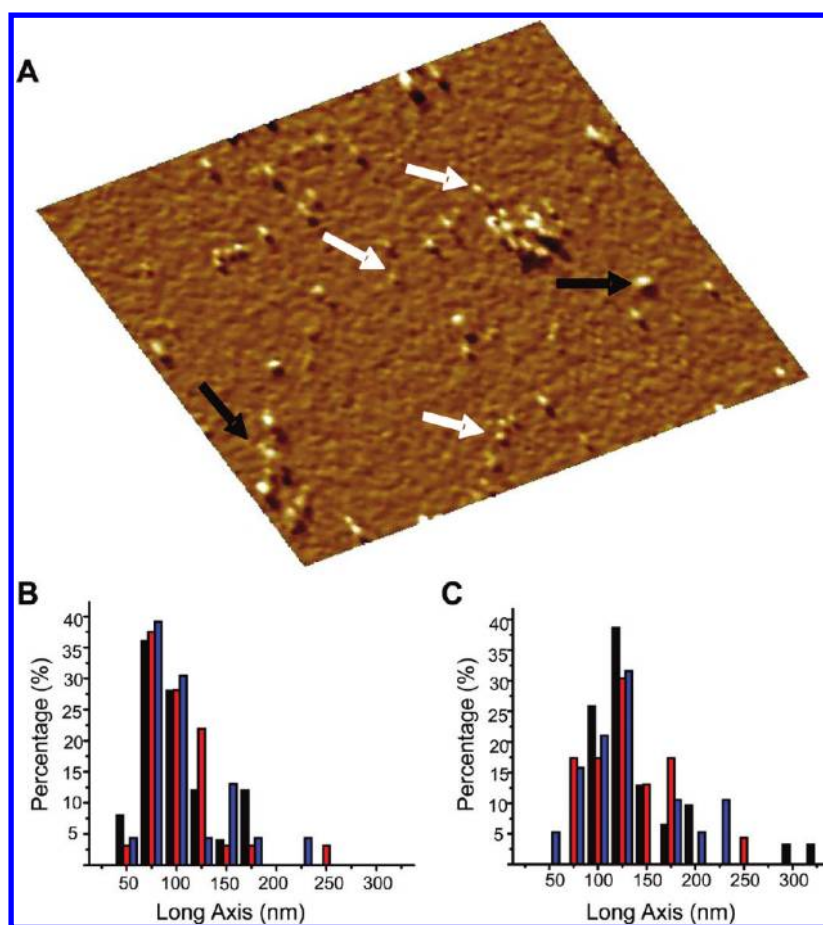


Figure 1. (A) AFM amplitude image (area $402 \times 402 \text{ nm}^2$) of freshly dissolved all D-amino acids $A\beta_{1-42}$ in PBS without Ca^{2+} or Mg^{2+} at $t = 0$ of time-lapsed imaging of the peptide. White arrows show peptides with heights of 1 to 2 nm, consistent with the size of monomers. Black arrows show higher order oligomers and clusters. The freshly cleaved mica surface was imaged in PBS solution alone to confirm zero contamination. The peptide was added to the PBS solution directly on the AFM stage to a final concentration of $\sim 35 \mu\text{g/mL}$ and the adsorbed peptide was imaged within 45 min. The length distribution of the long axis of the oligomers was measured for (B) all D-amino acids $A\beta_{1-42}$ and (C) all L-amino acids $A\beta_{1-42}$ isomers. In panel B, the colors indicate: black for 1.5 h ($n = 25$, here n denotes the number of oligomers), red stripes for 5 h ($n = 32$), and blue for 23 h ($n = 23$). In panel C, the colors indicate: black for 1.5 h ($n = 31$), red stripes for 6 h ($n = 23$), and blue for 25 h ($n = 19$). There is little change in distribution for both isomers, indicating stability of the oligomers.

Gly29.³⁰ In the latter conformer, two C-terminal residues, Ile41 and Ala42 were added to create $A\beta_{1-42}$.

The coordinates of all D-amino acids $A\beta_{1-42}$ are mirror-imaged coordinates of all L-amino acids $A\beta_{1-42}$ and can be obtained by reflecting the coordinates with respect to the reference plane. To simulate D-amino acids, a protein force field for asymmetric isomers is required. The standard CHARMM force field has been designed for L-amino acids. However, it can be directly used for D-amino acids because a D-amino acid is a mirror-image of an L-amino acid. Therefore, we adapted the same standard parameters to D-amino acids as those used for the L-amino acids. However, the parameters include the dihedral angle cross term map (CMAP), which for D-amino acids needs to be corrected because the map was constructed for L-amino acids.³⁷ Therefore, in our simulation, we corrected CMAP for D-amino acids by reflecting the phi-psi CMAP matrix for L-amino acids.

For construction of the β -barrel structure, both D- and L- $A\beta_{1-42}$ (each with two conformers) were inclined $\sim 37^\circ$ relative to the pore axis²¹ and then rotated 18 times with respect to the pore axis, creating $A\beta$ barrels (Figure S1 of the Supporting Information). The construction follows known structures of β -barrel membrane proteins such as those in the outer

membranes of bacteria, mitochondria, and chloroplasts, which have 8–22 β -strands with shear numbers ranging from 8 to 24, yielding a β -strand tilt angle range of 36 to 44° relative to the barrel axis.^{38,39} The $A\beta$ barrels were then embedded in an anionic lipid bilayer containing 1,2-dioleoyl-*sn*-glycero-3-phosphoserine (DOPS) and 1-palmitoyl-2-oleoyl-*sn*-glycero-3-phosphoethanolamine (POPE). A unit cell containing two layers of lipids was constructed. An anionic lipid bilayer, composed of DOPS/POPE (mole ratio 1:2) containing a total of 420 lipids, constitutes the unit cell with TIP3P waters added at both sides. For a given number of lipid molecules, the optimal value of lateral cell dimensions can be determined. The bilayer system containing an $A\beta$ barrel, lipids, salts, and waters has almost 190 000 atoms. For the bilayer construction, we closely follow previous β -sheet channel simulations.^{17–22,30}

The CHARMM program⁴⁰ using the revised CHARMM27 (C27r) force field for lipids⁴¹ and the modified TIP3P water model⁴² was used to construct the set of starting points and to relax the systems to a production-ready stage. A series of minimizations were performed for the initial configurations to remove overlaps of the alkane chains in the lipids and to relax the solvents around the $A\beta$ barrel gradually, which was held rigid. The initial configurations were gradually relaxed through

dynamic cycles with electrostatic cutoffs (12 Å). In the subsequent pre-equilibrium stages, a series of dynamic cycles were performed with the harmonically restrained peptides in the channels, and then the harmonic restraints were gradually diminished until gone with the full Ewald electrostatics calculation. The entire pre-equilibration cycle took 5 ns to yield the starting point. A Nosé–Hoover thermostat/barostat was used to maintain constant temperature of 303 K. The simulations for the preequilibrations and production runs were performed on the NPAT (constant number of atoms, pressure, surface area, and temperature) ensemble. Production runs of 100 ns for the starting points with the NAMD code⁴³ on the Biowulf cluster (<http://biowulf.nih.gov>) at the NIH was used for the starting point with the same CHARMM27 force field.⁴⁰ Averages were taken after 20 ns discarding initial transients.

Comparison with Other Models. Recently, the $A\beta_{1-42}$ channel was also modeled into 36-mer β -barrel channels.⁴⁴ These consisted of a hexamer-of-hexamers; that is, six β -barrels each consisting of six monomers, yielding a complex of exactly 36 monomers. The transmembrane pores were proposed to form between the hexamers' barrels. The β -barrels of six hexamers span the bilayer, merging to form a 36-stranded β -barrel. In this model, two 12-stranded parallel β -barrels formed by the N-terminal domain of $A\beta_{1-42}$ are located symmetrically at both extramembranous bilayer leaflets, and six parallel β -strands wrap around each β -barrel. In the membrane core, 24 β -strands containing the central residues (17–21) line an inner antiparallel β -barrel forming a solvated pore, and the C-terminal domain forms an outer 36-stranded antiparallel β -barrel interacting with lipids. This 36-mer barrel complex differs from our $A\beta$ barrel in size (being considerably larger than ours), complexity (it is more complex), $A\beta$ monomer conformation, barrel organization with respect to the bilayer (as described above), and its size uniqueness. (The channel always consists exactly of hexamer-of-hexamers, that is, 36 monomers, whereas our channels are dynamic in consideration of bilayer fluidity, and thus varied channel sizes as the loosely associated subunits associate/dissociate.) However, both models share similar residues that are engaged in a lipid-contacting outer barrel and the solvated pore. We emphasize that as always, modeling only provides models; eventually, any modeling requires direct, high-resolution experimental data. In the case of amyloids, given the heterogeneous landscape, we can expect a range of polymorphic channels.⁴⁵

RESULTS

D- $A\beta_{1-42}$ Forms Stable Globular Units. Both D- and L- $A\beta_{1-42}$ form oligomeric structures and these structures remain stable during the imaging by the AFM for up to a 23–25 h period. Within the first 45 min of AFM imaging after the addition of the peptide we saw mostly monomers approximately 1–2 nm in height and small oligomeric clusters (Figure 1A). The amount of oligomeric clusters increased successively over time though no structural changes were apparent over the 23–25 h time period. Significantly, we found this pattern for both D- and L- $A\beta_{1-42}$ peptides.

We measured the long axis of the oligomers and globular species at each time point for both isomers. We found the distribution for the D- $A\beta_{1-42}$ oligomers to remain similar throughout the observation period (Figure 1B). Similarly, the length distribution of the L- $A\beta_{1-42}$ oligomers measured along their long axis, remained stable from the initial time point, at 1.5 h, throughout the ~24 h observation period (Figure 1C). It

has been shown that many factors, including concentration, affect the fibril formation kinetics.⁴⁶ In our time-lapsed study, different concentrations were used for the D- $A\beta_{1-42}$ (~35 $\mu\text{g}/\text{mL}$) and the L- $A\beta_{1-42}$ (~13 $\mu\text{g}/\text{mL}$) peptides; therefore, the total extent of oligomerization over the observation period cannot be strictly compared between isomers. We observed the stability of the D- and L-isomers to be similar over similar time periods under similar ambient conditions.

D- $A\beta_{1-42}$ Forms Fibrils. Fibril formation of the $A\beta_{1-42}$ peptide incubated in ultrapure water at 37 °C for 72 h was studied in vitro to evaluate the kinetics and hierarchy of fibril structure for L- and D- $A\beta_{1-42}$.^{31,46,47} We found the fibril formations for both isomers to be indistinguishable after 72 h of incubation (Figure 2A,B). Both isomers form a complex network of fibers, protofibrils, and oligomers. In both images, globular complexes can be identified as well as fiber-like complexes exhibiting varied widths and lengths.

Aliquots of both isomers after 72 h of incubation were diluted several times to identify and measure the width of individual fibrils (Figure 2A,B (insets)). Numerous mature fibers had lengths greater than the maximum scan area ($5 \times 5 \mu\text{m}^2$) achievable with the scanner used for these experiments and therefore could not be measured accurately. Random measurements of fibril widths were taken and deconvoluted.^{31–33} We calculated the histograms of the distribution of fibril widths for both isomers (Figure 2C). The D-isomer (gray bars) and the L-isomer (black bars) show fibers with widths most frequently between 25 and 30 nm. The D-isomer shows a slight bias toward thicker fiber formation. 43.2% of the D-isomer width measurements were between 25 and 35 nm. The L-isomer showed a comparable but slightly lower distribution of width measurements with 49.1% of the measurements between 20 and 30 nm. The D-isomer and the L-isomer both show local minimum frequencies of width measurements just below these respective maximum ranges. The D-isomer local minimum frequency is between 20 and 25 nm, and the L-isomer local minimum frequency is between 15 and 20 nm.

D- $A\beta_{1-42}$ Forms Channels in Bilayers Characteristic of L- $A\beta_{1-42}$. The channel formation of D- $A\beta_{1-42}$ was investigated by imaging the pores formed in supported lipid bilayers of DOPC. The DOPC lipids were chosen for their low transition temperature and consistency with previously reported evidence of $A\beta_{1-42}$ pore formation by AFM studies and MD simulations.^{14,16–22,48} The bilayer sample preparation was optimized using the L-isomer to repeat and confirm previously reported results.^{14,16} The sample preparation process was repeated exactly for the D-isomer, and channels were consistently and repeatedly observed. We imaged pore-like structures in bilayer membrane by first finding the edge of the bilayer (with usual height of >5 nm with respect to the mica substrate plane) and sequentially minimizing the scan area to obtain a high-resolution image of the bilayer surface. This approach ensures that the features observed were characteristic of the bilayer and inserted peptide and not due to contamination of the mica surface. Control DOPC bilayers were imaged in high resolution in the absence of the peptide, and no pore-like topography was observed.

The D- $A\beta_{1-42}$ peptide forms channels in DOPC bilayers with a varying number of subunits (Figure 3A–C), structurally indistinguishable from the L- $A\beta_{1-42}$ channels (Figure 3D). The pores are heterogeneous, presenting trimers, tetramers, pentamers, and hexamers, with tetramers being the most

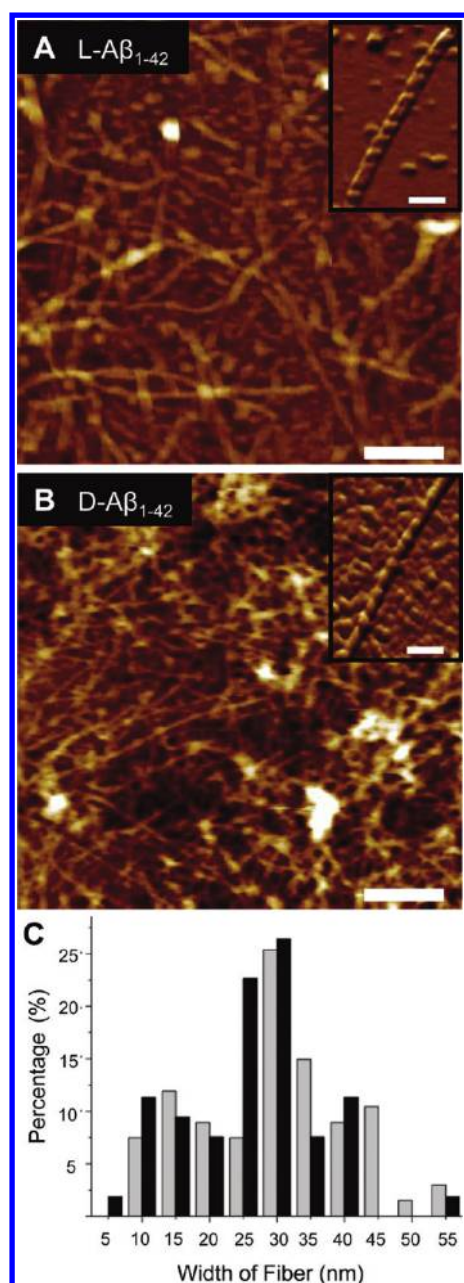


Figure 2. (A) L- and (B) D- $A\beta_{1-42}$ isomers induced toward fibril formation in the absence of a lipid membrane by incubation in 1% NH_4OH at 37 °C for 72 h, dried overnight on fresh mica, and imaged with AFM in air. Both isomers form similar complex networks of globular units, oligomers, protofibrils, and fibrils. Insets show high-resolution images of individual fibers (scale bars = 250 nm, height color scales = 25 nm, inset scale bars = 100 nm). (C) Distribution of randomly measured widths ($n = 67$, here n denotes the number of samples) of fibers of the D- $A\beta_{1-42}$ fibers (gray bars) after incubation at 37 °C for 72 h shows a distribution with fiber widths most frequently between 25 and 30 nm. The distribution of the L- $A\beta_{1-42}$ fibril widths (black bars), after similar incubation, also shows a distribution ($n = 53$) with fiber widths most frequently between 25 and 30 nm. The overall range of values is comparable for both isomers.

prevalent observed structures (Figure 3E). Pores were identified by the presence of individual segments forming a circular group in the amplitude image, coinciding with a small height increase with respect to the bilayer membrane surface in the AFM height image. Because of the larger size of the AFM

tip compared with the typical inner diameters of ion channels (~ 1 nm), the AFM images only provide information relating to depths which are in close proximity of the lipid bilayer/solution interface and cannot discern whether the individual annular structures actually traverse the entire thickness of the lipid bilayer. However, functional evidence provided by electrophysiological experiments with lipid bilayers reconstituted with $A\beta_{1-42}$ peptides suggests the presence of conductive pores, able to allow the selective passage of ions.^{14,16,30}

The inherent tendency of amyloid peptides to adopt the β -sheet conformation leads to the formation of a complex β -barrel-like channel structure composed of several β -sheet subunits in the membrane, where lipids promote the β -sheet formation.^{49–51} In our previous simulations, we modeled two truncated $A\beta$ barrels, $A\beta_{17-42}$ (p3), and $A\beta_{9-42}$ (N9),²¹ using U-shaped peptides with the β -strand-turn- β -strand motif.^{34,35} To model the full sequence $A\beta_{1-42}$ barrels, we again employ the U-shaped peptides as the membrane embedded portion and adopt the N-terminal structure from the $A\beta_{1-16}$ (coordinates taken from PDB code: 1ZE7)³⁶ as the extramembranous portion. Therefore, two $A\beta_{1-42}$ conformers define the turn: at Ser26-Ile31 (Conformer 1) and at Asp23-Gly29 (Conformer 2). Using these conformers, we constructed the D- and L- $A\beta_{1-42}$ isomer barrels and performed 100 ns explicit MD simulations on the $A\beta$ barrels embedded in an anionic lipid bilayer composed of DOPS/POPE (mole ratio 1:2). During the simulations, the $A\beta$ barrels are gradually relaxed through the interaction with surrounding lipids (Figure S2 of the Supporting Information). Whereas small fluctuations in the membrane embedded portions including the pore and C-terminal strands strongly preserve the U-shaped structure in the $A\beta$ barrels, large fluctuations convert the N-terminal strands to disordered chains in the bulk water area (Figure 4). In the $A\beta$ barrels, the fluctuation of the individual peptide's dynamics is inhomogeneous, although the dynamic motions for some adjacent peptides are correlated to each other (Figure S3 of the Supporting Information). We note that the MD simulations employed the anionic lipid bilayer composed of DOPS/POPE, and the AFM experiments used the zwitterionic lipid bilayer with DOPC; however, the results are expected to relate. In our modeling, the peptides are preinserted into the membrane core and assembled to form a channel. Under these circumstances, the hydrophobic interactions between lipid-facing residues in the channel and lipid tails should be an important factor to stabilize the channel conformation, and formation of the subunits in the channel structure may not completely rely on the interaction with the negatively charged PS lipid headgroups. Furthermore, in our previous simulations, we compared the subunits in the channel conformations for the p3 ($A\beta_{17-42}$) and N9 ($A\beta_{9-42}$) channels, when embedded in zwitterionic DOPC and in anionic POPC/POPG lipid bilayers, and observed no significant differences between the two.^{18,22} Therefore, our results with the anionic bilayer are expected to display the essential characteristics of $A\beta_{1-42}$ channels in the zwitterionic bilayers.

The molecular mass of our 18-mer $A\beta$ barrel is ~ 81.2 kDa, which is in the intermediate range of the $A\beta$ channels.^{18,22} The outer/pore diameters of our simulated barrels are $\sim 7.8/\sim 1.9$ and $\sim 8.2/\sim 2.1$ nm for the conformer 1 and 2 D- $A\beta_{1-42}$ barrels and $\sim 8.3/\sim 2.2$ and $\sim 8.1/\sim 2.0$ nm for the conformer 1 and 2 L- $A\beta_{1-42}$ barrels, respectively. The sizes measured for the barrels largely depend on the number of peptides composing the $A\beta$ barrels and partially depend on the location of the

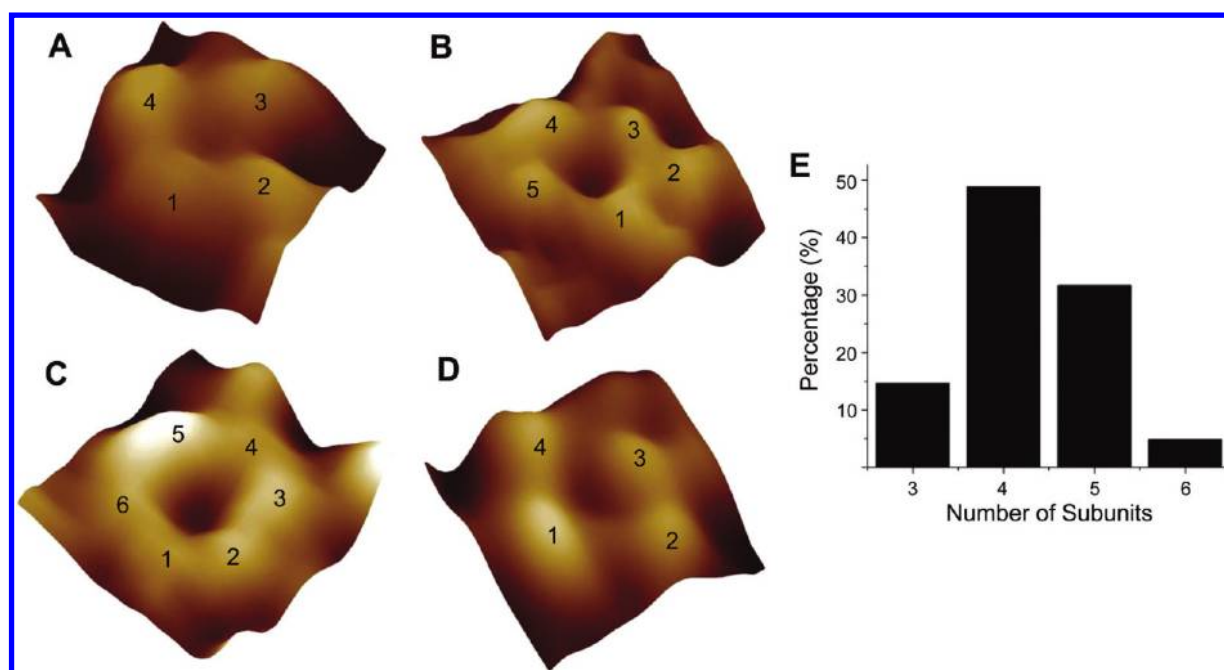


Figure 3. (A–C) AFM images of individual D- $A\beta_{1-42}$ channels in high resolution. Channels are resolved in the error mode image, seen here. These channels are heterogeneous and were observed as trimeric (not shown), (A) tetrameric, (B) pentameric, and (C) hexameric subunits assemblies. The channels formed by D- $A\beta_{1-42}$ are indistinguishable from the previously reported L- $A\beta_{1-42}$ channels. (D) An example AFM image of the L- $A\beta_{1-42}$ channels from the current study is shown. Channels are not observed in the absence $A\beta_{1-42}$ peptide. Image sizes are 11.5 nm for (A), 18.1 nm for (B), 13.2 nm for (C), and 14.4 nm for (D). (E) The distribution of channels formed by a varying number of $A\beta_{1-42}$ subunits. Channels with 3, 4, 5, or 6 subunits were observed. The most common structure is the channel with four subunits.

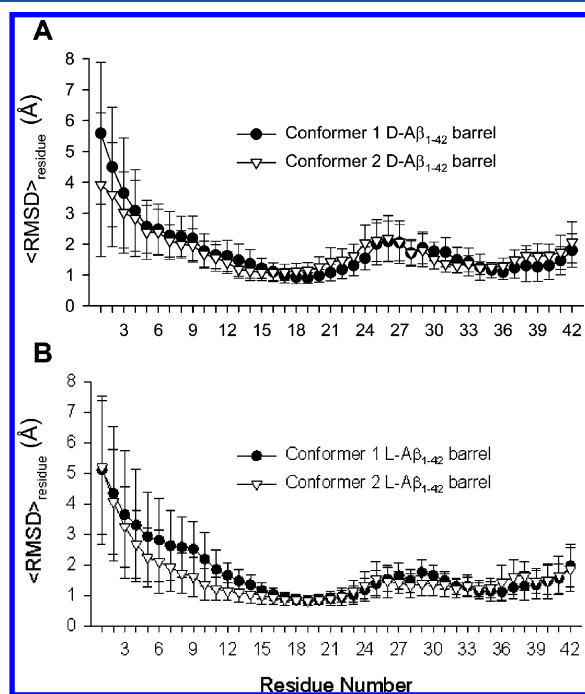


Figure 4. Residue averaged root-mean-squared deviation, $\langle \text{rmsd} \rangle_{\text{residue}}$, from the starting point for C_{α} atoms of the peptides for the (A) conformer 1 and 2 D- $A\beta_{1-42}$ barrels and the (B) conformer 1 and 2 L- $A\beta_{1-42}$ barrels.

extramembranous N-terminal portions. The N-terminal strands containing several charged residues stretch toward the lipid headgroups. The strong electrostatic interactions can increase the channel size; alternatively, they can interact with each other at the channel mouth blocking the entry into the pore. We

speculate that the interactions of the N-terminal strands near the channel mouth may correlate with features of calcium selective amyloid channels and zinc blockage. The 18-mer simulations obtained three to five subunits in the anionic bilayer (Figure 5). As we noted in our previous simulations, subunit formations result from the fluidic lipid bilayer dynamics, and even the same channel sizes may break into different number of subunits.^{17–22} To determine the subunits, we calculated the parameters, including the percentage of β -sheet content based on the intermolecular backbone hydrogen bonds (H-bonds), the β -strand order parameter, and the description of secondary structure, using our previous protocol (Figure S4 of the Supporting Information). Both D- and L-isomer $A\beta$ barrels present a range of sizes and morphologies similar to the imaged AFM channels. No difference is found between D- and L- $A\beta_{1-42}$ barrels, suggesting that both $A\beta_{1-42}$ isomers form ion channels in the lipid membrane, and thus $A\beta$ toxicity can take place in the absence of stereospecific interactions.

DISCUSSION

We have studied the formation of channel-like structures using all D-amino acids $A\beta_{1-42}$ and its chiral opposite, the all L-amino acids $A\beta_{1-42}$. We imaged indistinguishable pore structures formed by both isomers. Because the imaging was carried out in a lipid bilayer composed of DOPC lipids and without any inserted membrane receptors, we infer that the channel formation by the peptides in the membrane does not depend on stereospecificity. Moreover, the formation of channels in the absence of the negatively charged phosphatidylserine (PS) phospholipids as used in previous studies²⁷ indicates that once inserted into the membrane, $A\beta_{1-42}$ does not rely on a

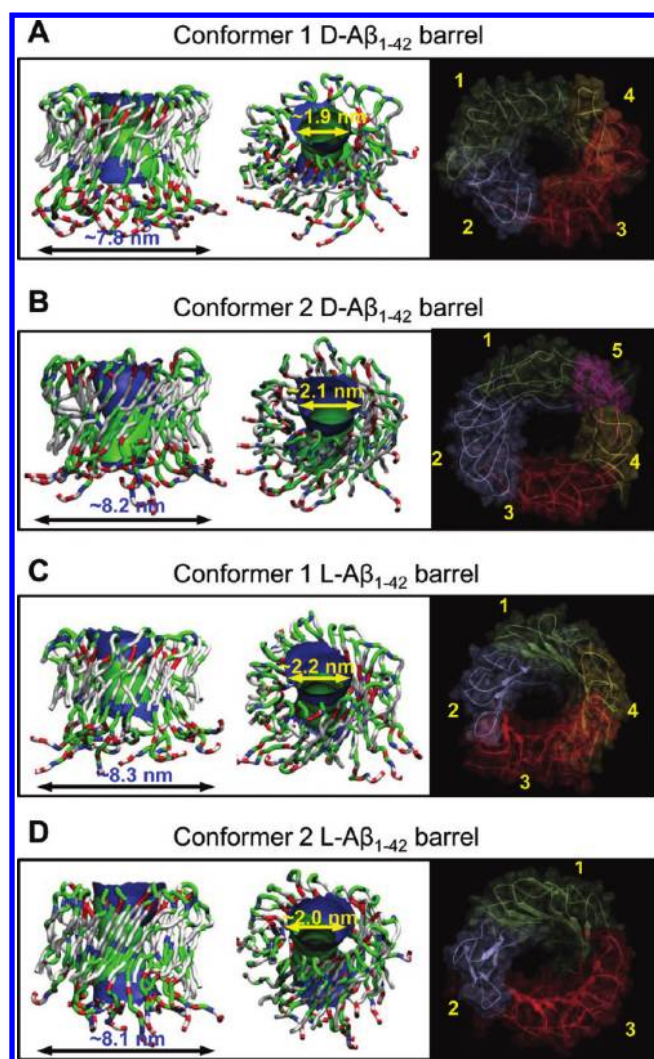


Figure 5. Averaged pore structures calculated by the HOLE program⁵⁵ embedded in the averaged barrel conformations during the simulations for the (A) conformer 1 and (B) 2 D- $A\beta_{1-42}$ barrels and the (C) conformer 1 and (D) 2 L- $A\beta_{1-42}$ barrels. In the side (left) and angle (middle) views of the pore structure, whole barrel structures are shown with the ribbon representation. In the peptide, hydrophobic residues are shown in white, polar and Gly residues are shown in green, positively charged residues are shown in blue, and negatively charged residues are shown in red. For the pore structures in the surface representation, red denotes pore radius of $r < 0.9$ nm, green denotes pore radius in the range, $0.9 \text{ nm} \leq r \leq 1.1$ nm, and blue denotes pore radius of $r > 1.3$ nm. The simulated barrel structures (right) with highlighted subunits for the averaged barrels in the surface representation are shown in the view along the membrane normal.

stereospecific interaction with PS to form the segmented channel structure.

On the basis of the structure–function relationship characteristics of peptides, we reasoned that the physicochemical behavior of the all D-amino acids enantiomer of $A\beta_{1-42}$ will be identical to the naturally occurring all L-amino acids, if the structural and kinetic behavior of $A\beta_{1-42}$ is independent of chirality. Time-lapse imaging of D- $A\beta_{1-42}$ on mica showed that under appropriate physiological conditions, immediately after the addition of freshly dissolved peptides, monomeric and oligomeric clusters are present and are stable over periods of time of ~ 23 h. Therefore, these 3D structural units are characteristic of those present during the formation of pores in

the presence of a lipid membrane. The physicochemical behavior of D- $A\beta_{1-42}$ in the time-lapsed study was similar to that of the previously reported behavior of L- $A\beta_{1-42}$, which was also confirmed in this study.⁵² We observed the formation of $A\beta_{1-42}$ fibers and larger oligomers after 72 h of incubation at 37 °C in 1% NH_4OH . Both isomers exhibited a similar distribution of widths of fibers. The similar maximum frequency widths preceded by local minimum frequency widths is likely due to the amyloid fibers' tendency to form hierarchical fibrillar structures.^{31,53} The D-enantiomer of $A\beta_{1-42}$ showed comparable physicochemical behavior to the L-enantiomer, with monomeric and oligomeric forms stable over short periods of incubation at room temperature in physiological buffer and fiber formation over long time periods at 37 °C in ultrapure water. Therefore, the species available for channel formation in the preparation of the supported lipid membrane are monomers and oligomers but not fibers.

Previous studies on the toxicity D- and L- $A\beta_{1-42}$ enantiomers presented conflicting results. Ciccotosto et al. reported $A\beta_{1-42}$ toxicity through receptor interaction with the PS lipid flipped to the extracellular side of the lipid bilayer.²⁷ Cribbs et al. asserted that L- and D- $A\beta_{1-42}$ show no difference in cellular toxicity.²⁹ Both studies focused on the binding of $A\beta_{1-42}$ to the cell membrane and the subsequent toxicity through fluorescence and viability assays. Neither study identified the mechanism of the toxicity, such as fibril adhesion, channel formation, oxidative stress, and so on.^{27,29} In our study, we focused on peptide insertion and channel formation with ion conductive pores in an effort to elucidate this path of toxicity, and our results show that both L- and D-isomers form characteristic channels in supported lipid bilayer.

A number of cell membrane receptors that can bind to $A\beta$, whether in monomeric or fibrillar form, have been discussed and summarized by Verdier et al.⁵⁴ Our current data as well as our previous experiments and MD simulations performed with model membranes reconstituted with $A\beta$ peptides in a receptor-free environment,^{14,16,20,30} show pore-like structural features and functional activity suggestive of an ion channel conductive mechanism that does not depend on the presence of cell receptors. However, because of the very nature of these model systems, they cannot rule out the action of cell receptor mechanisms in the complex cellular environment relevant to the disease.

CONCLUSIONS

In summary, we have studied the structure of channels in the lipid membrane as well as fibril formation in solution by the naturally occurring L- $A\beta_{1-42}$ peptide and its chiral opposite, the D- $A\beta_{1-42}$ enantiomer. We show that the two isomers exhibit indistinguishable pore structures, consistent with the MD results, and similar fibril formation behavior and stability. Previously we have shown that the D- $A\beta_{1-42}$ analog conducts ions, also in a manner indistinguishable from the L- $A\beta_{1-42}$ peptides.³⁰ Therefore, it is likely that insertion and toxic channel formation of $A\beta_{1-42}$ does not occur through a stereospecific interaction but by a direct pathway – through an ion channel.

ASSOCIATED CONTENT

Supporting Information

Monomer conformations and the initial barrel structures of MD simulations in ribbon and surface representations of all D-amino acids $A\beta_{1-42}$ peptides, time series of averaged peptide

interaction energy with DOPS and POPE lipids, peptide-averaged root-mean-squared deviation, and examples of parameters to define the subunits for the conformer 1 D- $\alpha\beta_{1-42}$ barrel. This material is available free of charge via the Internet at <http://pubs.acs.org>.

AUTHOR INFORMATION

Corresponding Author

*Tel: 301-846-5579, E-mail: ruthnu@helix.nih.gov (R.N.). Tel: (858) 822-0384, E-mail: rlal@ucsd.edu (R.L.)

Author Contributions

[†]Both authors contributed equally to this work.

ACKNOWLEDGMENTS

This research was supported by the National Institutes of Health (National Institute on Aging AG028709 to R.L.). This project has been funded in whole or partially with Federal funds from the National Cancer Institute, National Institutes of Health, under contract number HHSN261200800001E. This research was supported (partially) by the Intramural Research Program of the NIH, National Cancer Institute, Center for Cancer Research. All simulations had been performed using the high-performance computational facilities of the Biowulf PC/Linux cluster at the National Institutes of Health, Bethesda, MD (<http://biowulf.nih.gov>).

REFERENCES

- Temussi, P. A.; Masino, L.; Pastore, A. *EMBO J.* **2003**, *22*, 355.
- Dobson, C. M. *Nature* **2003**, *426*, 884.
- Selkoe, D. J. *Nature* **2003**, *426*, 900.
- Revesz, T.; Ghiso, J.; Lashley, T.; Plant, G.; Rostagno, A.; Frangione, B.; Holton, J. L. *J. Neuropathol. Exp. Neurol.* **2003**, *62*, 885.
- Neet, K. E.; Thinakaran, G. *J. Biol. Chem.* **2008**, *283*, 29613.
- Kang, J.; Lemaire, H. G.; Unterbeck, A.; Salbaum, J. M.; Masters, C. L.; Grzeschik, K. H.; Multhaup, G.; Beyreuther, K.; Muller-Hill, B. *Nature* **1987**, *325*, 733.
- Suzuki, N.; Cheung, T. T.; Cai, X. D.; Odaka, A.; Otvos, L. Jr.; Eckman, C.; Golde, T. E.; Younkin, S. G. *Science* **1994**, *264*, 1336.
- Walsh, D. M.; Klyubin, I.; Fadeeva, J. V.; Cullen, W. K.; Anwyl, R.; Wolfe, M. S.; Rowan, M. J.; Selkoe, D. J. *Nature* **2002**, *416*, 535.
- Hardy, J.; Selkoe, D. J. *Science* **2002**, *297*, 353.
- Arispe, N.; Rojas, E.; Pollard, H. B. *Proc. Natl. Acad. Sci. U.S.A.* **1993**, *90*, 567.
- Pollard, H. B.; Rojas, E.; Arispe, N. *Ann. N.Y. Acad. Sci.* **1993**, *695*, 165.
- Bhatia, R.; Lin, H.; Lal, R. *FASEB J.* **2000**, *14*, 1233.
- Rhee, S. K.; Quist, A. P.; Lal, R. *J. Biol. Chem.* **1998**, *273*, 13379.
- Lin, H. A. I.; Bhatia, R.; Lal, R. *FASEB J.* **2001**, *15*, 2433.
- Kourie, J. I.; Shorthouse, A. A. *Am. J. Physiol.* **2000**, *278*, C1063.
- Quist, A.; Doudevski, I.; Lin, H.; Azimova, R.; Ng, D.; Frangione, B.; Kagan, B.; Ghiso, J.; Lal, R. *Proc. Natl. Acad. Sci. U.S.A.* **2005**, *102*, 10427.
- Jang, H.; Zheng, J.; Nussinov, R. *Biophys. J.* **2007**, *93*, 1938.
- Jang, H.; Arce, F. T.; Capone, R.; Ramachandran, S.; Lal, R.; Nussinov, R. *Biophys. J.* **2009**, *97*, 3029.
- Jang, H.; Zheng, J.; Lal, R.; Nussinov, R. *Trends Biochem. Sci.* **2008**, *33*, 91.
- Jang, H.; Arce, F. T.; Ramachandran, S.; Capone, R.; Azimova, R.; Kagan, B. L.; Nussinov, R.; Lal, R. *Proc. Natl. Acad. Sci. U.S.A.* **2010**, *6538*.
- Jang, H.; Arce, F. T.; Ramachandran, S.; Capone, R.; Lal, R.; Nussinov, R. *J. Mol. Biol.* **2010**, *404*, 917.
- Jang, H.; Arce, F. T.; Ramachandran, S.; Capone, R.; Lal, R.; Nussinov, R. *J. Phys. Chem. B* **2010**, *114*, 9445.
- Kagan, B. L.; Azimov, R.; Azimova, R. *J. Membr. Biol.* **2004**, *202*, 1.
- Arispe, N.; Pollard, H. B.; Rojas, E. *Proc. Natl. Acad. Sci. U.S.A.* **1993**, *90*, 10573.
- Demuro, A.; Smith, M.; Parker, I. *J. Cell Biol.* **2011**, *195*, 515.
- Verdier, Y.; Penke, B. *Curr. Protein Pept. Sci.* **2004**, *5*, 19.
- Ciccotosto, G. D.; Tew, D. J.; Drew, S. C.; Smith, D. G.; Johanssen, T.; Lal, V.; Lau, T.-L.; Perez, K.; Curtain, C. C.; Wade, J. D.; Separovic, F.; Masters, C. L.; Smith, J. P.; Barnham, K. J.; Cappai, R. *Neurobiol. Aging* **2011**, *32*, 235.
- Lacor, P. N.; Buniel, M. C.; Furlow, P. W.; Clemente, A. S.; Velasco, P. T.; Wood, M.; Viola, K. L.; Klein, W. L. *J. Neurosci.* **2007**, *27*, 796.
- Cribbs, D. H.; Pike, C. J.; Weinstein, S. L.; Velazquez, P.; Cotman, C. W. *J. Biol. Chem.* **1997**, *272*, 7431.
- Capone, R.; Jang, H.; Kotler, S. A.; Connolly, L.; Arce, F. T.; Ramachandran, S.; Kagan, B. L.; Nussinov, R.; Lal, R. *J. Chem. Theory Comput.* **2012**, submitted for publication.
- Arimon, M.; Diez-Perez, L.; Kogan, M. J.; Durany, N.; Giral, E.; Sanz, F.; Fernandez-Busquets, X. *FASEB J.* **2005**, *19*, 1344.
- Relini, A.; Torrasa, S.; Ferrando, R.; Rolandi, R.; Campioni, S.; Chiti, F.; Gliozzi, A. *Biophys. J.* **2010**, *98*, 1277.
- Jang, H.; Arce, F. T.; Mustata, M.; Ramachandran, S.; Capone, R.; Nussinov, R.; Lal, R. *Biophys. J.* **2011**, *100*, 1775.
- Lührs, T.; Ritter, C.; Adrian, M.; Riek-Loher, D.; Bohrmann, B.; Doeli, H.; Schubert, D.; Riek, R. *Proc. Natl. Acad. Sci. U.S.A.* **2005**, *102*, 17342.
- Petkova, A. T.; Yau, W. M.; Tycko, R. *Biochemistry* **2006**, *45*, 498.
- Zirah, S.; Kozin, S. A.; Mazur, A. K.; Blond, A.; Cheminant, M.; Segalas-Milazzo, I.; Debey, P.; Rebuffat, S. *J. Biol. Chem.* **2006**, *281*, 2151.
- Mackerell, A. D.; Feig, M.; Brooks, C. L. *J. Comput. Chem.* **2004**, *25*, 1400.
- Schulz, G. E. *Biochim. Biophys. Acta* **2002**, *1565*, 308.
- Marsh, D.; Pali, T. *Biophys. J.* **2001**, *80*, 305.
- Brooks, B. R.; Brucoleri, R. E.; Olafson, B. D.; States, D. J.; Swaminathan, S.; Karplus, M. *J. Comput. Chem.* **1983**, *4*, 187.
- Klauda, J. B.; Brooks, B. R.; Mackerell, A. D. Jr.; Venable, R. M.; Pastor, R. W. *J. Phys. Chem. B* **2005**, *109*, 5300.
- Durell, S. R.; Brooks, B. R.; Bennaïm, A. *J. Phys. Chem.* **1994**, *98*, 2198.
- Phillips, J. C.; Braun, R.; Wang, W.; Gumbart, J.; Tajkhorshid, E.; Villa, E.; Chipot, C.; Skeel, R. D.; Kale, L.; Schulten, K. *J. Comput. Chem.* **2005**, *26*, 1781.
- Shafir, Y.; Durell, S.; Arispe, N.; Guy, H. R. *Proteins* **2010**, *78*, 3473.
- Miller, Y.; Ma, B.; Nussinov, R. *Chem. Rev.* **2010**, *110*, 4820.
- Antzutkin, O. N. *Magn. Reson. Chem.* **2004**, *42*, 231.
- Harper, J. D.; Lieber, C. M.; Lansbury, P. T. Jr. *Chem. Biol.* **1997**, *4*, 951.
- Arce, F. T.; Jang, H.; Ramachandran, S.; Landon, P. B.; Nussinov, R.; Lal, R. *Soft Matter* **2011**, *7*, 5267.
- Thundimadathil, J.; Roeske, R. W.; Guo, L. *Biopolymers* **2006**, *84*, 317.
- Kagan, B. L.; Thundimadathil, J. *Adv. Exp. Med. Biol.* **2010**, *677*, 150.
- Zhao, L. N.; Chiu, S.-W.; Benoit, J.; Chew, L. Y.; Mu, Y. *J. Phys. Chem. B* **2011**, *115*, 12247.
- Kowalewski, T.; Holtzman, D. M. *Proc. Natl. Acad. Sci. U.S.A.* **1999**, *96*, 3688.
- Ionescu-Zanetti, C.; Khurana, R.; Gillespie, J. R.; Petrick, J. S.; Trabachino, L. C.; Minert, L. J.; Carter, S. A.; Fink, A. L. *Proc. Natl. Acad. Sci. U.S.A.* **1999**, *96*, 13175.
- Verdier, Y.; Zarandi, M.; Penke, B. *J. Pept. Sci.* **2004**, *10*, 229.
- Smart, O. S.; Goodfellow, J. M.; Wallace, B. A. *Biophys. J.* **1993**, *65*, 2455.